Comput Mech
DOI 10.1007/s00466-012-0801-z

ORIGINAL PAPER

Computational homogenization of porous materials of Green type

Felix Fritzen · Samuel Forest · Djimedo Kondo · Thomas Böhlke

Received: 27 June 2012 / Accepted: 23 September 2012

Abstract The constitutive response of porous materials is investigated computationally. For the solid phase elasto-plastic behavior of Green type is considered, i.e. an isotropic compressible yield criterion is assumed. A wide range of material parameters and porosities from 0.1 to 30 % are investigated by means of FEM simulations of periodic ensembles of spherical pores. The dilatation of the pores and of the compressible matrix are evaluated. It is found that a large part of the total dilatation is due to plastic volume changes of the solid phase. The asymptotic stress states of the simulations are compared to analytical predictions by Shen et al. (Comput Mater Sci 62:189–194, 2012). Based on the computational data, an effective constitutive law is proposed and verified by means of additional computations. A three-scale homogenization procedure for double porous materials is proposed that depends only on the micro- and mesoscale porosity and the yield stress of the solid phase.

F. Fritzen (✉)
YIG Computer Aided Material Modeling, Chair for Continuum Mechanics, Karlsruhe Institute of Technology, Kaiserstr 10, Bldg.10.23, 76131 Karlsruhe, Germany
e-mail: felix.fritzen@kit.edu

S. Forest
Centre des Matériaux, UMR7633, Ecole des Mines de Paris /CNRS, BP 8791003 Evry Cedex, France

D. Kondo
Institut Jean le Rond d'Alembert, Université Pierre etMarie Curie, Boîte 162, Tour 55–65, 4 Place Jussieu, Paris Cedex, 75252 05 France

T. Böhlke
Chair for Continuum Mechanics, Institute of Engineering Mechanics, Karlsruhe Institute of Technology, Karlsruhe, Germany
e-mail: thomas.boehlke@kit.edu

Keywords Computational homogenization · Porous materials · Three-scale homogenization · Plastic compressibility · Material of Green type

1 Introduction

The investigation of the macroscopic yield surface of microporous materials is a subject with a rich history. Following the pioneering studies by [21] and by [14,31] developed a limit analysis approach for the derivation of a macroscopic criterion of ductile porous media. This approach, which considers a rigid plastic matrix, is mainly based on the use of a simple trial velocity field leading to an upper bound of the macroscopic yield stress as a function of the applied pressure. This pressure dependency is noteworthy as the matrix material itself is considered incompressible. On the basis of unit cell calculations [38], later modified the Gurson criterion by introducing some adjusting parameters. The subsequent so-called GTN model [39] is still now extensively used in literature for the prediction of the effects of void growth on the structural response of metallic parts in the context of isotropic ductile damage. To overcome well known basic drawbacks of the original Gurson model, in particular at low stress triaxialities, a limit analysis based extension has been carried out by [11] who considered a refined velocity field inspired from the elastic solution of the hollow sphere problem. Still in the same spirit [23,25], considered an Eshelby-type velocity field, which was shown to provide significant modifications of the original Gurson criterion. These modifications proved to be efficient in structural analysis, as shown by [18]. An extensive computational study has recently been presented by [10] in which three-dimensional porous volume elements were considered in finite element simulations in order to investigate the accuracy of the

Published online: 16 October 2012

previously mentioned analytical methods. The therein provided data was also intended to serve for the validation of subsequently proposed analytical methods.

Approaching the subject from a different point of view [28], has proposed a nonlinear variational homogenization approach for ductile porous materials. This approach has been interpreted later and shown to be equivalent to the so-called modified secant moduli method [36]. Though, it appears to provide too stiff predictions at large stress triaxialities, the variational approach leads to good results at low stress triaxialities. In order to improve this nonlinear homogenization model the more accurate second-order method was introduced by [3,5,6]. They proposed more accurate models for porous materials allowing in particular to recover the Gurson one at purely hydrostatic loadings. The recent proposal of [4] can further account for anisotropic pore morphologies and the evolution of the pore shape.

In spite of their great scientific and practical interest, all the above-cited studies considered porous materials with a von Mises type solid matrix and do not account for matrix plastic compressibility. However, such compressibility characterizes various engineering materials among which geomaterials, polymers or double porous materials can be mentioned. For ductile porous materials having a matrix which obeys to the Drucker–Prager criterion, a number of studies extending the Gurson approach has been proposed in literature [see also 13,15,16][1]. Implementation and application of the subsequent constitutive models have been recently done by [18]. Note that the macroscopic yield function obtained by [13] and used in these last studies allows to recover the Gurson criterion when the matrix becomes plastically incompressible. Other extensions of the Gurson approach, accounting for plastic compressibility, have been also proposed by [17] [see also the recent work of 24] in the case of a Mises–Schleicher solid matrix criterion (see [19][2] and also [29,30] for practical interest). Note also that, as the Drucker–Prager one, the Mises–Schleicher criterion of the matrix material exhibits an asymmetry between tension and compression.

Moreover, let us emphasize that for double porous media, plastic compressibility is also a central point of the modeling [e.g., 40], even when the solid phase at the lowest scale is incompressible. Mainly motivated by application to double porous media [34,35], recently derived, by means of a Gurson-type approach, a class of macroscopic criteria. It corresponds to a porous material having a matrix obeying to an elliptical, more precisely a Green type, criterion. They also presented the application of their analytical result to double porous media. The main objective of the present study is to assess the criterion established by these authors by numerically investigating a representative volume element composed of a matrix material of Green type and spherical cavities. The paper extends the methodology used previously for plastically incompressible materials [10] in order to investigate the effect of the compressibility of the matrix material of porous aggregates. Such a systematic analysis of random porous material with compressible matrix is not available in the literature yet. It can serve as a basis for the construction and identification of effective constitutive equations for double porous materials.

The paper is organized as follows. First, the geometrical modeling and discretization of the microstructure is briefly described, as well as the constitutive law of the matrix material and the loading conditions. A convenient parametrization of the microstructural constitutive parameters is given. In Sect. 3 the results of the asymptotic stress response obtained from the approximately 2,000 finite element simulations are presented as well as selected local stress and strain fields. As the matrix material is plastically compressible the part of the volume change due to the actual pore volume change is analyzed and compared to the volume change of the bulk material. The pressure sensitivity of the macroscopic yield stress is compared to the analytical predictions of [35]. Section 4 is devoted to the identification and validation of an effective constitutive model based on the computational data.

In Sect. 5 the proposed criterion is applied to the three-scale homogenization of double porous materials with incompressible solid phase at the smallest scale.

1.1 Notation

An index free notation is used with lowercase symbols denoting scalars, e.g. c, ψ, ϕ, lowercase bold face letters denoting first-order tensors (or vectors), e.g. $\boldsymbol{x}$, $\boldsymbol{u}$, and uppercase Latin and lowercase Greek bold face letters representing second-order tensors, e.g. $\boldsymbol{A}$, $\boldsymbol{\sigma}$, $\boldsymbol{\varepsilon}$. Fourth-order tensors are typeset as $\mathbb{C}$, $\mathbb{A}$ or $\mathbb{P}$. Based on the identity on symmetric second-order tensors $\mathbb{I}^{\mathrm{s}}$ and the second-order identity tensor $\boldsymbol{I}$ the two isotropic projectors are defined by

$$\mathbb{P}_1 = \frac{1}{3}\boldsymbol{I} \otimes \boldsymbol{I}, \quad \mathbb{P}_2 = \mathbb{I}^{\mathrm{s}} - \mathbb{P}_1. \tag{1}$$

The Euclidean norm is denoted as $\| \bullet \|$ and $\boldsymbol{a} \cdot \boldsymbol{b}$, $\boldsymbol{A} \cdot \boldsymbol{B}$ represent the standard inner products for vectors and tensors, respectively. Arguments of functions such as the position $\boldsymbol{x}$ or time t are omitted for brevity if not explicitly required in the given context. For convenience, we define the spatial averaging operator over the volume element Ω_{tot} as

[1] Note also the contribution by Maghous et al. [20] who has implemented and originally developed for a Drucker–Prager matrix the variational method of Ponte Castañeda [28].

[2] The original publication of this pressure-dependent criterion can be found in [32]

$$\langle \bullet \rangle = \frac{1}{|\Omega_{\text{tot}}|} \int_{\Omega} \bullet \, \mathrm{d}V. \tag{2}$$

Here Ω is the part of Ω_{tot} occupied by solid material, i.e. Ω_{tot} without the voids. In an Euclidean basis spanned by the orthonormal vector basis $\{\boldsymbol{e}_1, \boldsymbol{e}_2, \boldsymbol{e}_3\}$, the matrix of the components of a tensor is written as

$$[\boldsymbol{A}] = \begin{pmatrix} A_{11} & A_{12} & A_{13} \\ A_{21} & A_{22} & A_{23} \\ A_{31} & A_{32} & A_{33} \end{pmatrix}, \; A_{ij} = \boldsymbol{A} \cdot \boldsymbol{e}_i \otimes \boldsymbol{e}_j. \tag{3}$$

2 Modeling

2.1 Constitutive assumptions

In the following we are concerned with the macroscopic behavior of isotropic porous materials with non-overlapping cavities. No hardening is considered in order to be able to identify asymptotic stress states. The latter have often been the basis of analytical limit analysis based models for porous materials and they have given rise to accurate predictions [see also 10, for a comparison to computational findings]. A linear kinematic description is assumed with the infinitesimal strain tensor $\boldsymbol{\varepsilon}$ defined as the symmetric displacement gradient. For the investigated materials the scale separation hypothesis is assumed to hold and a two scale description is used.

The smaller scale (microscale) denotes the scale at which the matrix material is considered homogeneous and the geometry of the pores is accounted for. The macroscopic (or structural) scale denotes the level at which the porous materials are usually employed. For these applications, the influence of the microstructural physical and geometrical heterogeneity on the effective constitutive material response are the aim of homogenization methods in general. Details regarding the three scale homogenization based to the two scale description presented here are provided in Sect. 5.

In the following the macroscopic domain is denoted $\bar{\Omega}$ and the microscopic domain in which the pores are actually represented is referred to by Ω, as illustrated in Fig. 1. The boundary $\partial\mathscr{P}$ of the pores $\mathscr{P}$ is assumed to be traction free, i.e. the surface of the pores is a free boundary with zero traction vector $\boldsymbol{t} = \boldsymbol{\sigma}\boldsymbol{n} = \boldsymbol{0}$, where $\boldsymbol{n}$ denotes the unit normal vector pointing out of the pores. The considered volume element Ω_{tot} of the material is taken as a cube in which the matrix $\Omega \subsetneq \Omega_{\text{tot}}$ and the voids $\mathscr{P} = \Omega_{\text{tot}} \setminus \Omega$ are placed. In the given setting the microscopic and macroscopic stress and strain tensors are related by [see, e.g., 26]

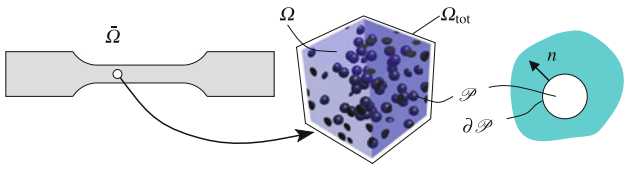

Fig. 1 Illustration of the two scale problem

$$\bar{\boldsymbol{\varepsilon}} = \frac{1}{|\Omega_{\text{tot}}|} \int_{\Omega} \boldsymbol{\varepsilon} \mathrm{d}V + \bar{\boldsymbol{\varepsilon}}_{\text{c}} = (1-f)\langle \boldsymbol{\varepsilon} \rangle_{\Omega} + \bar{\boldsymbol{\varepsilon}}_{\text{c}}, \tag{4}$$

$$\bar{\boldsymbol{\varepsilon}}_{\text{c}} = \frac{1}{|\Omega_{\text{tot}}|} \int_{\mathscr{P}} \text{sym}(\boldsymbol{u} \otimes \boldsymbol{n}) \mathrm{d}A, \tag{5}$$

$$\boldsymbol{\Sigma} = \frac{1}{|\Omega_{\text{tot}}|} \int_{\Omega} \boldsymbol{\sigma} \mathrm{d}V = (1-f)\langle \boldsymbol{\sigma} \rangle_{\Omega}, \tag{6}$$

where $\bar{\boldsymbol{\varepsilon}}_{\text{c}}$ represents the effective cavity strain due to the deformation of the boundary of the pores and f denotes the pore volume fraction.

2.2 Microscopic constitutive model

The subsequent observations rely on an additive decomposition of the total strain tensor $\boldsymbol{\varepsilon}$ into an elastic part $\boldsymbol{\varepsilon}^{\text{e}}$ and a plastic part $\boldsymbol{\varepsilon}^{\text{p}}$ according to

$$\boldsymbol{\varepsilon} = \boldsymbol{\varepsilon}^{\text{e}} + \boldsymbol{\varepsilon}^{\text{p}}. \tag{7}$$

The elastic part of the strain determines the stress tensor via a positive definite fourth-order stiffness tensor $\mathbb{C}$

$$\boldsymbol{\sigma} = \mathbb{C}[\boldsymbol{\varepsilon}^{\text{e}}] = \mathbb{C}[\boldsymbol{\varepsilon} - \boldsymbol{\varepsilon}^{\text{p}}]. \tag{8}$$

The previous relation defines a generalized Hooke's law.

In the following $\mathbb{C}$ is isotropic. For the bulk modulus K and the shear modulus G it is given by

$$\mathbb{C} = 3K\mathbb{P}_1 + 2G\mathbb{P}_2. \tag{9}$$

The elastic material parameters used by [10] are assumed for consistency, i.e. a Young's modulus E of 200 GPa and a Poisson ratio ν of 0.3 which define K and G according to

$$K = \frac{E}{3(1-2\nu)}, \quad G = \frac{E}{2(1+\nu)}. \tag{10}$$

The elastic parameters are arbitrarily chosen and it has been verified, that variations do not influence the overall response of the material.

In the previous study [10] a von Mises type plasticity model was used for the matrix material. An intrinsic property of this material class is its plastic incompressibility. The present study considers a plastically compressible isotropic matrix materials which is based on an elliptic yield criterion also referred to as Green type plasticity model. For details

see the original formulation by [12], its application to powder metallurgy by [2], and more recently to metallic foams by [1,7]. Rate-independent behavior and the absence of hardening effects are assumed. Given the Cauchy stress tensor $\boldsymbol{\sigma}$ and non-negative parameters $C, F \geq 0$, an equivalent stress σ_{eq} can be defined by

$$\sigma_{\mathrm{eq}}(\boldsymbol{\sigma}; C, F) = \sqrt{\frac{3}{2} C \boldsymbol{\sigma}' \cdot \boldsymbol{\sigma}' + F \,\mathrm{tr}^2(\boldsymbol{\sigma})}, \tag{11}$$

where $\boldsymbol{\sigma}' = \boldsymbol{\sigma} - \frac{1}{3}\mathrm{tr}(\boldsymbol{\sigma})\boldsymbol{I}$ denotes the deviatoric stress tensor. Then a convex domain of admissible states is defined by

$$\varphi(\boldsymbol{\sigma}) = \sigma_{\mathrm{eq}}(\boldsymbol{\sigma}; C, F) - \sigma_0 \overset{!}{\leq} 0, \tag{12}$$

with $\sigma_0 > 0$ denoting the yield stress of the material. Referring to a simple scaling argument, a more convenient representation of (12) is given by

$$\varphi(\boldsymbol{\sigma}) = \sigma_{\mathrm{eq}}(\boldsymbol{\sigma}; 1, \tilde{F}) - \tilde{\sigma}_0, \quad \tilde{\sigma}_0 = \frac{\sigma_0}{\sqrt{C}}, \quad \tilde{F} = \frac{F}{C}. \tag{13}$$

The experimental identification of the parameters $\tilde{F}$ and $\tilde{\sigma}_0$ in experiments can be performed based on a deviatoric stress-driven loading which directly delivers $\tilde{\sigma}_0$ and subsequently an arbitrary loading at non-zero stress triaxiality in order to determine $\tilde{F}$. The possibility to keep track of the material parameters by standard experiments is an important property of the chosen model.

Based on the principle of maximum inelastic dissipation the rate of plastic deformation is

$$\dot{\boldsymbol{\varepsilon}}^{\mathrm{p}} = \dot{\zeta} \frac{\partial \varphi}{\partial \boldsymbol{\sigma}} = \frac{\dot{\zeta}}{\sigma_{\mathrm{eq}}} \left(\frac{3}{2} C \boldsymbol{\sigma}' + F \,\mathrm{tr}(\boldsymbol{\sigma})\, \boldsymbol{I} \right) \tag{14}$$

for $\dot{\zeta} \geq 0$ and $\dot{\zeta}\, \varphi(\boldsymbol{\sigma}) = 0$. The model includes the classical von Mises flow rule for the particular choice $\tilde{F} = 0$. For positive $\tilde{F}$ the plastic strain tensor has a volumetric component, i.e., plastic volume changes are explicitly allowed for. As pointed out by [9], uni-axial stress loading in $\boldsymbol{e}_2 \otimes \boldsymbol{e}_2$-direction induces the following plastic strain rate

$$[\dot{\boldsymbol{\varepsilon}}^{\mathrm{p}}] = \frac{\dot{\zeta}\, \mathrm{sign}(\sigma_{22})}{\sqrt{C + F}} \begin{pmatrix} F - C/2 & 0 & 0 \\ 0 & C + F & 0 \\ 0 & 0 & F - C/2 \end{pmatrix}. \tag{15}$$

In the limit case $F = C/2$ or $\tilde{F} = 1/2$ the plastic Poisson ratio ν_{p} defined via

$$\nu_{\mathrm{p}} = -\frac{\dot{\varepsilon}^{\mathrm{p}}_{11}}{\dot{\varepsilon}^{\mathrm{p}}_{22}} \tag{16}$$

is zero, meaning that there is no lateral plastic contraction for any uniaxial prescribed stress applied to the material. If $F > C/2$, then the plastic Poisson ratio becomes negative. The latter case is not considered in the subsequent investigations, although some geo-materials or particularly designed microstructres may show such behavior [e.g., 8, and references quoted therein].

The material model was implemented using a two-dimensional root finding problem. The unknowns are the increment in the deviatoric plastic strain and the increment in the volumetric strain. The non-linear equations consist then of the yield condition and a second equation enforcing the associative flow rule. This implementation is robust and provides a convenient notation of the tangent stiffness operator.

The ratio $\tilde{F} = F/C$ is an important material parameter determining the plastic compressibility of the material. In this paper different values of $\tilde{F}$ are investigated in order to cover a broad range of constitutive laws. A first set of parameters is obtained from a micro-mechanically motivated model of double porous materials with perfectly separated scales. In this case the model of [22] can be used to describe the constitutive behavior of the micro-porous material denoting the matrix material on the mesoscale. The parameters C and F depend on the micro-porosity f_μ according to

$$C(f_\mu) = \frac{1 + \frac{2}{3} f_\mu}{(1 - f_\mu)^2}, \quad F(f_\mu) = \frac{1}{4 \left(\ln\left(f_\mu\right)\right)^2}. \tag{17}$$

The micro-scale porosities f_μ =10, 25 and 40 % correspond to $\tilde{F} = F/C = 0.03581$, 0.06272 and 0.08463, respectively. These ratios are well below the limit case $\tilde{F}$ =0.5. In order to account for matrix materials at elevated porosities, e.g., open cell foams, the three artifical parameters $\tilde{F}$ =1/4, 3/8 and 1/2 are investigated to cover the admissible parameter range. In total this gives rise to the six different materials summarized in Table 1 that are used in the current study.

The computational cost associated with the numerical study is substantial due to the variation of the material parameters, the different loadings required to capture varying stress triaxilities and variations of the porosity. A major task is, hence, to make a well-reflected choice with respect to the examined porosities, the number of pores N and the number of statistical realizations of the microstructure N_{R}.

2.3 Geometrical modeling

Periodic microstructures consisting of boolean models of hard spheres representing the voids are used, where an isotropic distribution of the cavities is asserted. A detailed description with respect to the generation and analysis of the properties of the microstructures is given by [10]. Based on the investigations made for von Mises type matrix materials two conclusions are a priori drawn: (i) for very small volume fractions up to 1 % a single pore model appears appropriate and (ii) a number of N =50 pores within a single cuboidal

Table 1 Microscopic material properties of the solid phase assumed in the current study

E	200 (GPa)	ν	0.3	σ_0	100 (MPa)	
i	1	2	3	4	5	6
F_i	0.0472	0.1301	0.2978	0.250	0.375	0.500
C_i	1.317	2.074	3.519	1.000	1.000	1.000
$\tilde{\sigma}_0$ (MPa)	87.14	69.44	53.31	100	100	100
$\tilde{F}_i$	0.03581	0.06272	0.08463	0.250	0.375	0.500
$\tilde{C}_i$	1.000	1.000	1.000	1.000	1.000	1.000

Table 2 Geometry parameters used in the computational study

Type	f (%)	N	N_R
Single inclusion	0.1	1	1
Models	1.0	1	1
Periodic	5.0	50	10
Multi-pore	15	50	10
Models	30	50	10

f pore volume fraction, N number of pores, N_r number of realizations

volume can be considered sufficient, if the deviation of the overall response induced by different statistical realizations is not too large. Both assumptions can a posteriori be validated by means of exemplary computations. It is also noteworthy that periodic displacement fluctuation boundary conditions are essential to reduce the size of the reference volume element, i.e. the number of inclusions that need to be considered, in comparison to uniform kinematic boundary conditions. Note that no actual length can be associated to the unit cell, which would be the case for gradient enriched theories [see, e.g., 27].

In order to gain qualitative and quantitative information, three pore volume fractions are decided on for the multi-pore models containing 50 periodic spherical voids: f =5, 15 and 30 %. For each of these volume fractions N_R =10 different statistical realizations are considered in order to be able to judge on the statistical scatter due to the finite size of the volume element, i.e. to account for the limited number of inclusions. In addition to these ensembles, additional single pore models containing one void in the center of the unit cell at 0.1 and 1 % pore volume fraction are also considered. Table 2 provides an overview on the chosen geometrical models. In total, 32 different microstructures are generated.

Periodic spatial discretizations have been generated based on the periodic input geometry using the mesh generation tool `Netgen` [33]. In order to keep the computational cost as low as possible without loosing to many details, the results of the mesh density study provided in [10] are exploited. Isoparametric second-order tetrahedra are used. The number of degrees of freedom of the models varied between 200,000 and 350,000. Examples for the discretizations are shown in Fig. 2. With respect to the chosen discretization level it has been verified that the computational results show only minor variations of the effective material response when compared to calculations at finer resolution.

2.4 Loading conditions

Periodic displacement fluctuation boundary conditions are used. In order to circumvent the inherent disadvantages of stress controlled boundary conditions due to the constant yield stress, strain-driven boundary conditions of the type

$$\dot{[\bar{\boldsymbol{\varepsilon}}]} = \alpha \begin{pmatrix} 1 & 0 & 0 \\ 0 & -1 & 0 \\ 0 & 0 & 0 \end{pmatrix} + \beta \begin{pmatrix} 1 & 0 & 0 \\ 0 & 1 & 0 \\ 0 & 0 & 1 \end{pmatrix}. \tag{18}$$

are used, were α and β are parameters indirectly controlling the triaxiality of the stress state. Ten different loading conditions characterized by the tuples given in Table 3 are applied to each of the 32 microstructures and to each of the 6 different material models. These variations yield a total of $32 \times 6 \times 10 = 1{,}920$ different problems, which amount to a substantial computational effort given the non-linearity of the microscopic constitutive law and the geometric complexity of the models. The total computation time for the calculations was reduced by selection of a specific set of solver parameters for the parallel preconditioned conjugate gradient method used in order to solve the occuring linear systems. In addition to that a projection algorithm has been used to provide initial guesses for the iterative solution technique based on previously computed nodal displacement changes. Still the total computation time amounts to approximately 24,000 hours of CPU time (1,000 days). The computational time for one individual load case varied between 45 min. and 3 hours when using 8 CPUs.

3 Results

3.1 Asymptotic stress response

The assumed constant yield stress of the material allows to investigate the asymptotic material behavior of the

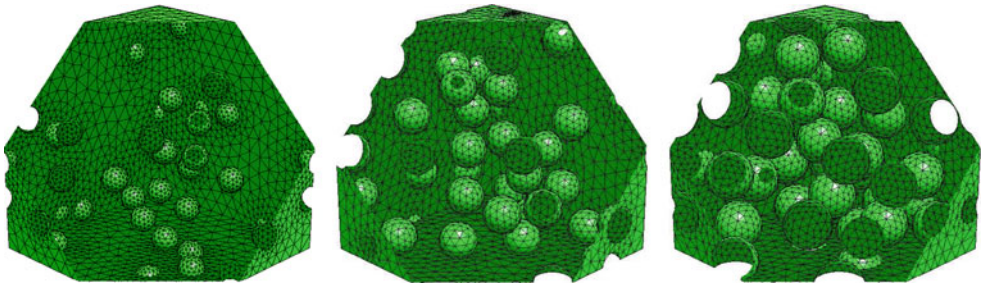

Fig. 2 Examples of the finite element discretizations at f =5 % (*left*), 15 % (*middle*) and 30 % (*right*) pore volume fraction

Table 3 Parameters for the ten different loading conditions

i	1	2	3	4	5	6	7	8	9	10
α_i	1.00	1.00	1.00	1.00	1.00	1.00	1.00	1.00	1.00	0.00
β_i	0.00	0.10	0.20	0.30	0.40	0.50	0.65	0.75	0.90	1.00

heterogeneous medium which is in correspondence to the results obtained by limit analysis [14]. In order to obtain the asymptotic constitutive response, the strain-driven loading has been continued to a level at which all of the following three characteristics remain numerically constant: (i) the macroscopic von Mises stress $\Sigma_{\mathrm{vM}} = \sqrt{3/2}\|\mathrm{dev}(\boldsymbol{\Sigma})\|$, (ii) the macroscopic hydrostatic stress $\Sigma_{\mathrm{m}} = 1/3\,\mathrm{tr}(\boldsymbol{\Sigma})$ and (iii) the macroscopic power density $\bar{P}$. The latter is computed based on the Hill-Mandel condition according to

$$\bar{P} = \frac{1}{|\Omega_{\mathrm{tot}}|}\int_{\Omega} \boldsymbol{\sigma}\cdot\dot{\boldsymbol{\varepsilon}}\,\mathrm{d}V = \boldsymbol{\Sigma}\cdot\dot{\bar{\boldsymbol{\varepsilon}}}. \tag{19}$$

The last computed stress field of each finite element computation is considered as the asymptotic stress response.

In order to represent the results of the computational study in a concise format, the common representation of the yield surface for isotropic porous materials showing the macroscopic von Mises equivalent stress Σ_{vM} as a function of the macroscopic hydrostatic stress state Σ_{m} is chosen. An additional normalization with respect to the microscopic yield stress $\tilde{\sigma}_0$ is performed as this parameter has basically no influence on the results as the elastic strains can be considered negligible in all simulations. The computational results for all five considered pore volume fractions f are shown in Figs. 3, 4, and 5 (f =1 %, 15 % omitted for brevity).

A major difference to the plastically incompressible von Mises material model can immediately be observed from Fig. 3. For such small porosities a material with incompressible matrix material, almost no sensitivity of the macroscopic deviatoric stress with respect to the hydrostatic stress state at low and intermediate stress triaxialities is observed in finite element simulations and analytical predictions [see, e.g., 10]. For the elliptic, i.e. compressible, matrix material used in the current investigations this is no longer the case. To be more precise, even small hydrostatic stresses have a notable

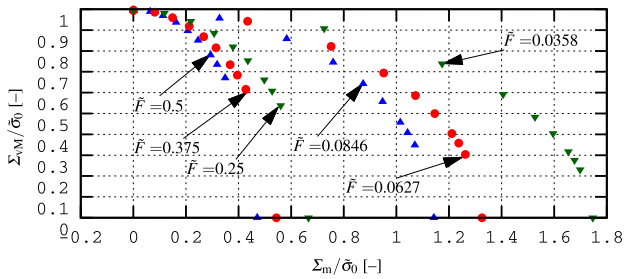

Fig. 3 Asymptotic stress response for a porosity f=0.1 % for the six different sets of material parameters (single pore model)

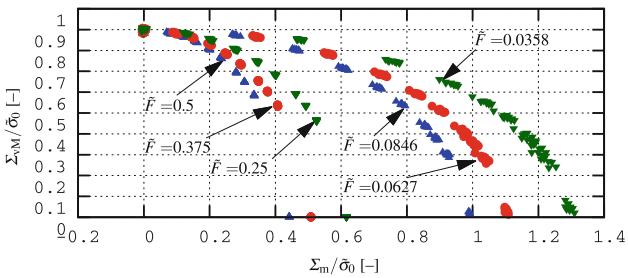

Fig. 4 Asymptotic stress response for a porosity f=5 % for the six different sets of material parameters

influence on the effective von Mises stress at which yielding occurs, even if the porosity is small. Additionally, the transition to the region in which the hydrostatic stress state dominates becomes smoother.

A second major observation is the massive influence of the microscopic material parameter $\tilde{F}$ on the maximum hydrostatic stress at which yielding occurs. Obviously the plastic compressibility of the matrix has a significant impact on the overall compressibility of the material.

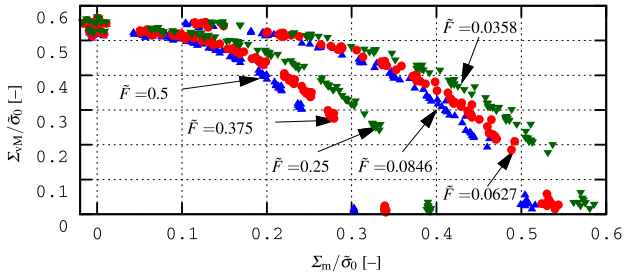

Fig. 5 Asymptotic stress response for a porosity f=30 % for the six different sets of material parameters

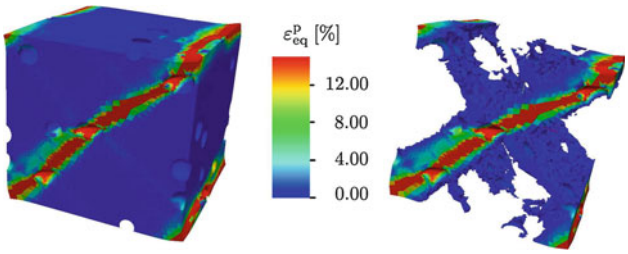

Fig. 6 Accumulated plastic strain at the end of the simulation for $\tilde{F}$ =0.5, f =5 % and deviatoric loading (α =1, β =0); *left* entire volume element, *right* regions with $\varepsilon^p_{eq} \geq 0.5\,\%$

3.2 Strain localization in the matrix material

The local fields of some of the calculations are investigated in order to compare the local plastic strain distribution for the elliptic Green type matrix material to results obtained using classical von Mises type plasticity. For the perfectly compressible matrix material ($\tilde{F}$ =0.5) the accumulated plastic strain

$$\varepsilon^p_{eq} = \int_0^T \|\dot{\boldsymbol{\varepsilon}}^p\| \mathrm{d}t \tag{20}$$

is shown in Fig. 6 for a porosity of 5 % and 50 voids. Besides a dominating shear band in the 45° direction, secondary perpendicular shear bands occur. These secondary shear bands occur preferably in regions with increased local porosity. Further investigations show that for the given loading only the regions surrounding the pores undergo a plastic dilatation whereas the remainder of the material obeys more or less to a classical von Mises plasticity model since $\mathrm{tr}(\boldsymbol{\sigma}) \approx 0$ holds.

When the loading is changed such that macroscopic volume changes occur, the situation is different. In Fig. 7 the loading is combined (α =1, β =0.50) in the left picture whereas it is purely volumetric, i.e. α =0 and β =1 in the right image. The pictures show regions in which the von Mises stress overpasses 90 % of the yield stress (left) and 33.3 % of the yield stress (right), respectively. It can be observed that for the combined loading interconnected regions around the pores exist in which the deviatoric stresses

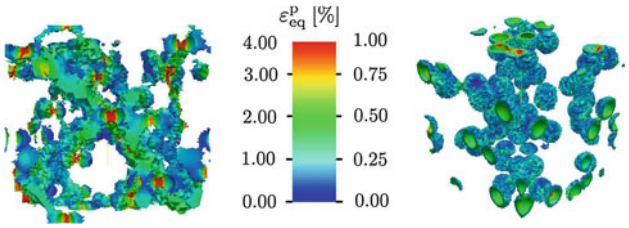

Fig. 7 Accumulated plastic strain at the end of the simulation for $\tilde{F}$ =0.5, f =5 %; *left* σ_{vM} >$0.9\tilde{\sigma}_0$ for combined loading (α =1, β =0.5); *right* σ_{vM} >$0.333\tilde{\sigma}_0$ for volumetric loading (α =0, β =1)

dominate the plastic deformation. These regions have a complex geometry, i.e. they are curved. For the volumetric loading it is found that basically all of the plastic deformation occurs due to hydrostatic stress states except for the immediate surrounding of the pores. As the pore boundary is the only region determining the actual cavity growth this observation implies that porosity changes induced by hydrostatic states are however mainly driven by isochoric plastic deformations. With respect to the investigation of the plastic volume changes in the matrix we refer to the following section.

3.3 Inelastic volume changes in the pores and the matrix

For plastically incompressible materials the determination of the pore growth is simple: any macroscopic volume change can be attributed to a growth of the cavities as the elastic volume changes can be neglected for most metallic materials. In the case of the elliptic yield criterion this is no longer true. The total dilatation ΔV_{tot} of the volume element can be partitioned into a dilatation due to elastic deformation of the matrix ΔV_e, a part due to the plastic dilatation of the matrix ΔV_{pl} and, finally, the part which is due to the actual cavity growth ΔV_g:

$$\Delta V_{tot} = \Delta V_e + \Delta V_p + \Delta V_g. \tag{21}$$

By normalization with respect to the volume of the cuboidal bounding box and with account for the constitutive model used in the calculations the following form is obtained

$$\mathrm{tr}(\bar{\boldsymbol{\varepsilon}}) = \frac{\mathrm{tr}(\boldsymbol{\Sigma})}{3K} + \frac{1}{|\Omega_{tot}|}\int_{\Omega} \mathrm{tr}(\boldsymbol{\varepsilon}^p)\mathrm{d}V + \Delta f. \tag{22}$$

It is known that for zero porosity, i.e. for a solid material, and non-zero $\tilde{F}$ all the volume change is due to the plastic compressibility of the matrix. For $\tilde{F} = 0$, the volume change is purely due to elastic deformations which are neglected in the present results. In the simulations we have found that the ratio of the volume change due to pore growth ΔV_g and the total volume change depend almost only on the porosity and the plastic compressibility parameter, but not on the applied loading. Therefore, the ratio has been averaged over all ten

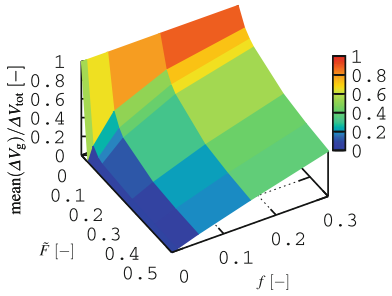

Fig. 8 Relative volume change due to pore growth with respect to the total volume change as a function of $\tilde{F}$ and the porosity f (values between the computational results are linearly interpolated)

loadings and over all realizations in order to get a robust estimate. The thereby obtained mean volume change due to the cavity growth with respect to the total volume change is plotted in Fig. 8. Note that in the absence of the pores no cavity growth takes place as void nucleation has been excluded from the current investigation. It can be noted that even for rather small values of the compressibility parameter $\tilde{F}$ a substantial amount of plastic deformation is attained due to plastic dilatation of the matrix which can amount for more than 90 % for low porosities.

3.4 Comparison to the model of Shen et al. (2012)

The homogenization of the properties of porous materials with spheroidal and ellipsoidal voids has been an active field of research for years. The extension to materials with elliptic yield surface has, however, only very recently been investigated by [35]. In the notation presented in Sect. 2 the effective yield criterion proposed by these authors reads

$$\varphi_*^{\text{Shen}}(\boldsymbol{\Sigma}) = \sqrt{\frac{\Sigma_{\text{vM}}^2 + 9\tilde{F}\Sigma_{\text{m}}^2 + 2f\tilde{\sigma}_0^2\cosh\left(\frac{3}{2}\frac{\Sigma_{\text{m}}}{\tilde{\sigma}_0}\right)}{1+f^2}} - \tilde{\sigma}_0 \tag{23}$$

where $\varphi_*^{\text{Shen}}(\boldsymbol{\sigma}) \leq 0$ has to be satisfied. The model of Shen and colleagues is identical to Gurson's model, except for the additional contribution due to the non-zero parameter $\tilde{F}$ that induces an additional drop of the effective von Mises stress in the presence of hydrostatic stresses. It is long known that Gurson's model can only provide accurate predictions for low porosities. Hence, the model given by (23) is a priori expected to provide accurate estimates for low porosities. With increasing porosity the deviations to the computational results are expected to get more important. No a priori knowledge on the accuracy in the presence of a non-zero parameter $\tilde{F}$ exists. In order to assess the accuracy of the effective yield criterion given by (23), the computational results of the current investigation are compared to the model predictions in Fig. 9.

The following conclusions can be drawn for the model proposed [35]:

- The accuracy of the model depends on both, the porosity f and the parameter $\tilde{F}$.
- With increasing porosity f the prediction looses accuracy.
- As the matrix material approaches plastic incompressibility, i.e. for small $\tilde{F}$, the deviations to the computational results get larger. In the limit case $\tilde{F} \to 0$ the model is identical to the classical Gurson model.
- The point on the hydrostatic axis is in good agreement even for porosities of 5 and 30 %, if $\tilde{F}$ is not too small.
- The prediction of yielding in the presence of purely deviatoric stress states is not accurately predicted for porosities larger than 5 % independent on the choice of $\tilde{F}$.

4 Effective constitutive behavior

4.1 Effective elliptic model

The aim of the current study is not the determination of a single set of effective material parameters or of one effective material law for a single set of parameters f, $\tilde{F}$, but it is sought after an effective constitutive behavior which includes all of the following material characteristics: the porosity f, the parameter $\tilde{F}$ and the microscopic yield stress $\tilde{\sigma}_0$ of the normalized yield condition (13). As has been shown in the previous section, the analytical approach of [35] by means of limit analysis is not capable to predict accurately the effective behavior in the presence of either large porosities or low plastic compressibility.

In other previous investigations with a matrix material that is plastically incompressible, the macroscopic yield criterion shows a pronounced pressure dependency. This implies a priori that in that case the microscopic material law of the matrix cannot be used as a candidate for a macroscopic criterion. In the case of elliptic material models with non-zero $\tilde{F}$, the microscopic material model is already compressible. This has motivated the attempt to find for given microscopic parameters $\tilde{F}$, $\tilde{\sigma}_0$ and for the porosity f the macroscopic parameters C_*, $F_* \geq 0$, such that

$$\varphi_*(\boldsymbol{\Sigma}) = \sigma_{\text{eq}}(\boldsymbol{\Sigma}; C_*, F_*) - \tilde{\sigma}_0 \leq 0 \tag{24}$$

is an accurate approximation of the asymptotic yield surface of the material. The effective parameters C_* and F_* are then functions of the pore volume fraction and of the microscopic parameter $\tilde{F}$:

$$C_* \equiv C_*(f, \tilde{F}), \quad F_* \equiv F_*(f, \tilde{F}). \tag{25}$$

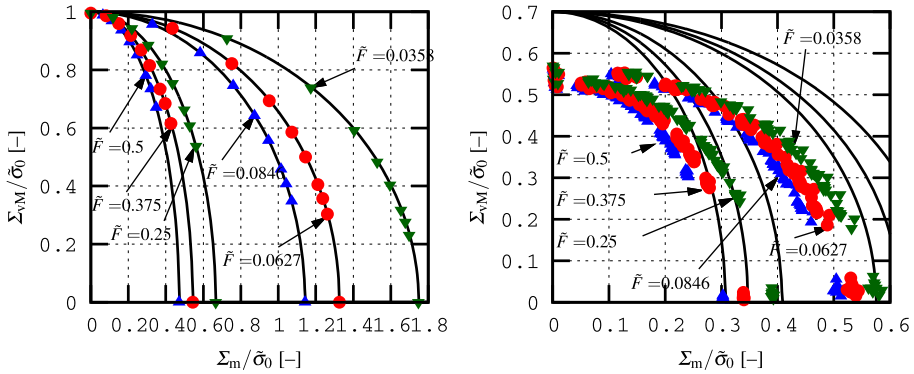

Fig. 9 Comparison of the computational data to the model of [35] (*left* 0.1 %, *right* 30 %)

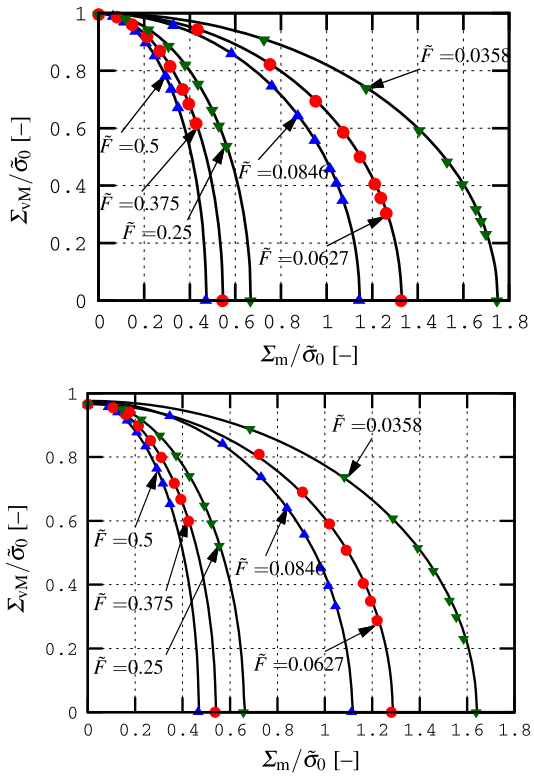

Fig. 10 Comparison of the determined elliptic material models with the computational values of the single pore models: f =0.1 % (*top*) and 1 % (*bottom*)

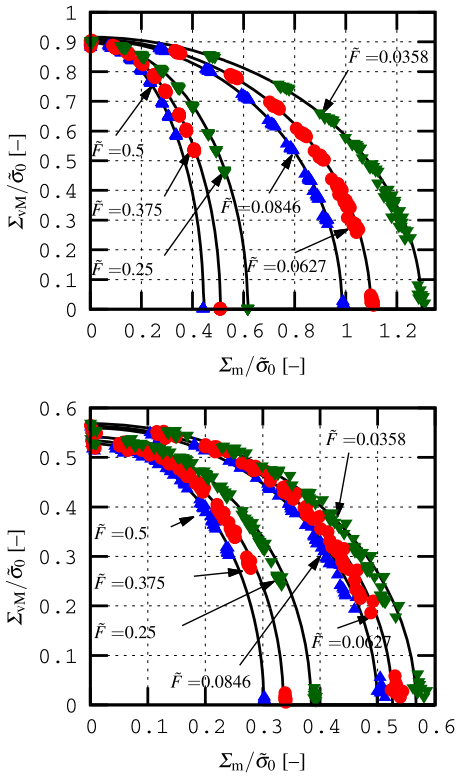

Fig. 11 Comparison of the determined elliptic material models with the computational values of the random microstructures: f =5 % (*top*) and 30 % (*bottom*)

For each of the in total 30 different curves (5 volume fractions and 6 values for $\tilde{F}$) the effective parameters C_* and F_* have been identified by means of a least square approximation resulting into a non-linear optimization problem. Although this approach appears simplistic, the comparison of the thereby predicted yield surfaces with the numerical results presented in Figs. 10 and 11 shows an excellent agreement between the computations and the proposed criterion (f =15 % omitted for brevity).

Using linear interpolation between the different values of the plastic compressibility parameter at constant f, three-dimensional graphs can be obtained, see Fig. 12 for an examples at $f = 5\,\%$ This representation shows that the dependency of the effective yield curve includes a coupling of the parameters f and $\tilde{F}$, i.e. the different three-dimensional representations are not self-similar.

It is found that at low porosities f the influence of the compressibility parameter $\tilde{F}$ is more pronounced than at higher pore volume fractions. This can be seen by comparison of the results of the constitutive models with f_μ =10 % (i.e. $\tilde{F} =$ 0.03581) and $\tilde{F} = 0.5$. Two important points in stress space are considered: the hydrostatic limit stress $\Sigma_{m,max}$ where

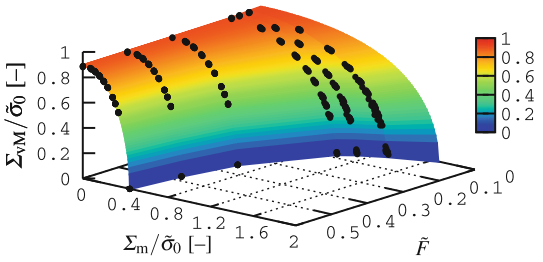

Fig. 12 Effective yield surface as a function of $\tilde{F}$ for f =5 %

Table 4 Sensitivity s_F (28) of the effective plastic compressibility parameter F_* as a function of the volume fractions

f (%)	0.1	1	5	15	30
s_F	3.706	3.506	2.921	2.308	1.876

Σ_{vM} is zero and the maximum von Mises stress $\Sigma_{vM,max}$ at vanishing macroscopic hydrostatic stress. Based on the proposed elliptic models these two stresses are

$$\Sigma_{m,max} = \tilde{\sigma}_0 \frac{1}{\sqrt{3F_*}}, \; \Sigma_{vM,max} = \tilde{\sigma}_0 \frac{1}{\sqrt{C_*}}. \tag{26}$$

Then the ratio

$$\kappa = \frac{\Sigma_{m,max}}{\Sigma_{vM,max}} = 3\sqrt{\frac{C_*}{F_*}} \tag{27}$$

is a measure of the plastic compressibility of the material. Moreover, the sensitivity of F_* with respect to $\tilde{F}$ at constant pore volume fraction f can be estimated by the ratio

$$s_F = \frac{\Sigma_{m,max}(\tilde{F}_{min})}{\Sigma_{m,max}(\tilde{F}_{max})} = \sqrt{\frac{F_*(f, \tilde{F}_{max})}{F_*(f, \tilde{F}_{min})}}. \tag{28}$$

The sensitivity s_F is given in Table 4 for all volume fractions. Note that C_* is almost independent of $\tilde{F}$. This implies that the yield stress under purely deviatoric loading is largely independent of the compressibility of the matrix material.

At 0.1 % pore volume fraction the influence of the parameter $\tilde{F}$ on the maximum hydrostatic stress is 3.71. The sensitivity steadily reduces to 1.88 for a porosity of 30 %. This is due to the two competing mechanisms causing the global volume change: the cavity growth and the plastic volume change of the matrix material. A discussion of this effect is presented in Sect. 3.3.

4.2 Prediction of the effective elliptic material parameters

Based on the 30 different sets of parameters C_* and F_* identified based on the computational data, the functions $C_*(\tilde{F}, f)$, $F_*(\tilde{F}, f)$ can be estimated using inter- and extrapolation.

The computational data can be enhanced by existing results in the following two limit cases:

- If the pore volume fraction vanishes then the effective material properties coincide with the microscopic ones, i.e. $C_*(f \to 0, \tilde{F}) = 1$ and $F_*(f \to 0, \tilde{F}) = \tilde{F}$.
- For plastically incompressible materials the adjusted Gurson Tvergaard Needleman (aGTN) model proposed by [10] is employed in order to identify $C_*(f, 0)$ and $F_*(f, 0)$ for arbitrary f (see Sect. 5 for details).

The range of admissible input arguments f and $\tilde{F}$ can be limited as for the considered class of microstructures relying on a boolean model of spheres the pore volume fraction f_{sat} at which saturation occurs is approximately 38 % [see, e.g., 37]. Hence, the porosity f is assumed in the range of 0 to 35 %. For $\tilde{F}$ values in the range from zero to one half are considered for the reasons given in Sect. 2.

First, C_* and F_* are determined as smooth functions of $\tilde{F}$ for each of the five pore volume fractions f_i ($i = 1, \ldots, 5$) considered in the simulations. Therefore, real valued parameters $p_{i1}, \ldots, p_{i4}$ and $q_{i1}, \ldots, q_{i4}$ are identified, such that

$$C_*(\tilde{F}, f_i) = p_{i1} + \frac{p_{i2}}{p_{i3} + \tilde{F}} + p_{i4}\tilde{F}, \tag{29}$$

$$F_*(\tilde{F}, f_i) = q_{i1} + \frac{q_{i2}}{q_{i3} + \tilde{F}} + q_{i4}\tilde{F} \tag{30}$$

are the least square approximation to the six parameters $C_*(\tilde{F}_j, f_i)$, $F_*(\tilde{F}_j, f_i)$ ($j = 1, \ldots, 6$) as functions of $\tilde{F}$.

The effective material parameters at arbitrary pore volume fraction f are then obtained by means of interpolation using the Lagrange polynomials

$$\phi_i(f) = \prod_{j \neq i} \frac{f - f_j}{f_i - f_j}, \tag{31}$$

with the values f_1 =0 %, f_2 =5 %, f_3 =15 % and f_4 =30 %. As the analytical results for zero porosity are known and high polynomial interpolations can lead to spurious oscillations, the two smallest volume fractions (f =0.1 and 1 %) are not considered for the interpolation. The approximations of the parameters of the effective elliptic yield criterion are

$$C_*(\tilde{F}, f) = \sum_{i=1}^{4} \phi_i(f) C_*(\tilde{F}, f_i), \tag{32}$$

$$F_*(\tilde{F}, f) = \sum_{i=1}^{4} \phi_i(f) F_*(\tilde{F}, f_i). \tag{33}$$

The simplicity of the approach and the wide range of possible input parameters render the presented interpolation function an interesting tool for the straight-forward application in non-linear computations containing porous materials with a matrix material exhibiting an elliptic yield surface. Note that the parameters identified from the computational results for 0.1 and 1 % porosity coincide with the interpolated values which is a confirmation of the chosen method. The parameters

Table 5 Parameters for the interpolation polynomials given by (32), (33)

i	f_i (%)	p_{i1}	p_{i2}	p_{i3}	p_{i4}
1	0	1	0	1	0
2	5	1.258767365924654	−0.007404878040900	0.100561171179904	−0.006768972199967
3	15	2.354849159226308	−0.439747868455195	0.658417984020198	−0.226639643143124
4	30	3.419782965408158	−0.042282472094084	0.089043013818485	0.514387319622058
i	f_i (%)	q_{i1}	q_{i2}	q_{i3}	q_{i4}
1	0	0	0	1	1
2	5	0.054116892687946	−0.544593295389388	20.689182103210008	1.071102643944395
3	15	0.117928608902041	−0.533800365294810	21.956516284245215	1.294809833103372
4	30	0.538361819649397	−0.271588390209856	1.048071178326330	1.717723039517716

p_{ij} and q_{ij} used to set up the interpolation are given in Table 5. An illustration of the interpolations for C_* and F_* is shown in Fig. 13. A relation of the parameters C_* and F_* to experimentally accessible values is given in terms of the maximum hydrostatic $\Sigma_{\mathrm{m,max}}$ and von Mises equivalent stress $\Sigma_{\mathrm{vM,max}}$ of the effective material according to (26).

In addition to the presented interpolations, a verification at a porosity of 24 % and with $\tilde{F}$=1/6 has been carried out in terms of additional finite element simulations. Again, 50 pores have been modeled, but only a single geometric realization is considered. All ten loadings described in Section 2 are applied to the volume element. The asymptotic stress response of these ten simulations is then compared to the effective elliptic yield criterion defined by the interpolation (32), (33) in Fig. 14. The point on the hydrostatic axis is underestimated by 2.8 % and the point at zero stress triaxiality is overestimated by 2.7 %. Remarkably the intermediate points at finite stress triaxiality are predicted almost to numerical precision. These results confirm the chosen interpolation technique since the chosen porosity f and plastic compressibility parameter $\tilde{F}$ are both in a range where few computational values are available and where the slope of the interpolations for C_* and F_* are important, i.e. the test case is considered a worst case scenario and errors are expected to be even smaller for other combinations of f and $\tilde{F}$.

5 Three-scale homogenization of double porous materials

In the present study the material law proposed by [22] was used in order to determine input parameters for the elliptic material model on a micromechanical basis and the assumption of a micro-scale porosity f_μ within the matrix material, see Fig. 15 for an illustration. This implies the existence of a third characteristic length scale besides the two length scales explicitly considered so far. This third length scale is assumed

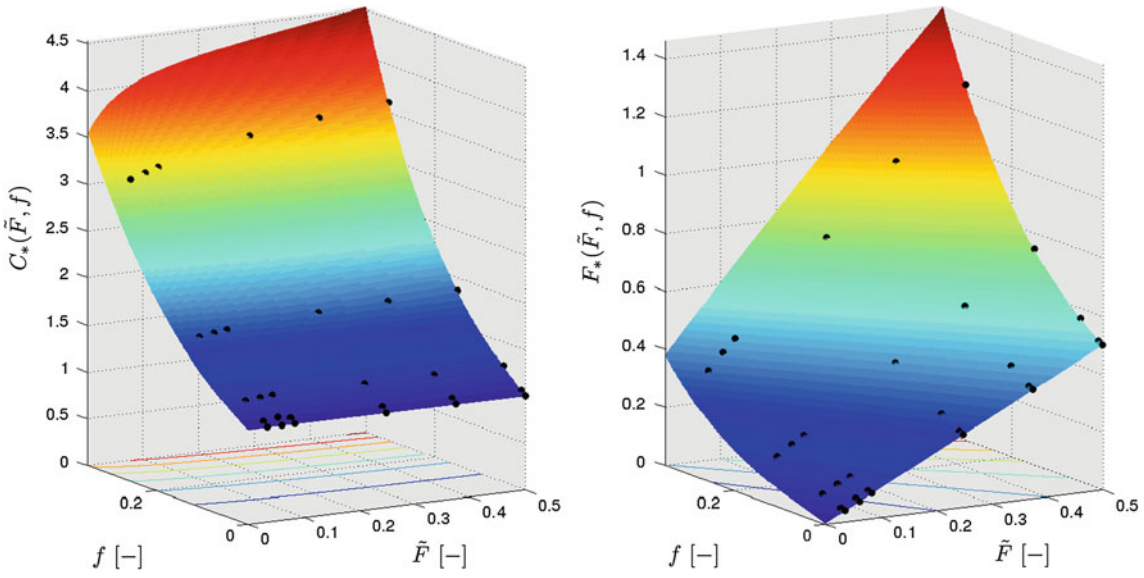

Fig. 13 Surface plots of C_*, F_* using (32),(33) for $f \in$[0,35 %], $\tilde{F} \in$[0, 0.5]); *dots* represent the parameters fitted to the computations

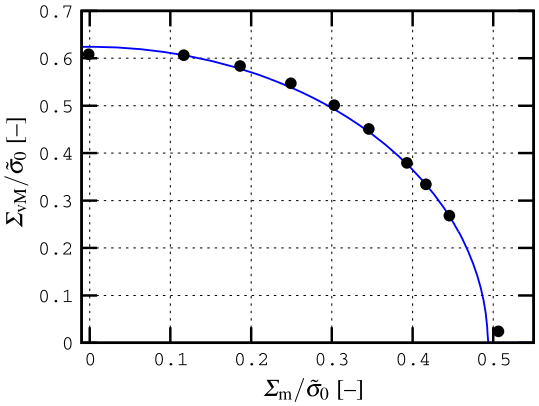

Fig. 14 Comparison of the asymptotic stress states obtained from the finite element simulations for f =24 %, $\tilde{F}$ =1/6 (points) to the effective yield criterion defined via the interpolation (32), (33)

to be clearly separated from the mesoscopic length scale, i.e. the pores found in the matrix have to be significantly smaller than the pores observed in the volume element calculations.

As is long known, the predictions of [22] are considered to give accurate estimates at low porosities and with deviations increasing along with the porosity f. Therefore the adjusted Gurson Tvergaard Needleman model was proposed by [10]

$$q_1(f) = \theta_0 - \theta_1 f, \quad q_2(f) = \theta_2, \quad q_3(f) = (q_1(f))^2, \tag{34}$$

$$\frac{\Sigma_{vM}}{\sigma_F} = \sqrt{1 + q_3(f) f^2 - 2 q_1(f) f \cosh\left(q_2(f) \frac{3\Sigma_m}{2\sigma_F}\right)}. \tag{35}$$

The parameters θ_0, θ_1, θ_2 are obtained from computational homogenization, f is the porosity and σ_F the yield stress of the matrix material. The aGTN model extends the GTN model by an additional dependence of the parameters on the porosity in order to account for increasing pore-pore interactions.

In order to define a new staggered homogenization scheme for the double porous material, the adjusted Gurson Tvergaard Needleman model (34), (35) can be approximated by an elliptic yield criterion that replicates the two important limit cases $\Sigma_{m,max}$ and $\Sigma_{vM,max}$ based on (26). The resulting parameters $\tilde{\sigma}_0(f_\mu)$ and $\tilde{F}(f_\mu)$ then determine the macroscopic yield criterion in the presence of the second size population of voids at a volume fraction f according to the interpolation (32), (33). Thereby, a closed form expression of the effective constitutive law of the non-linear three-scale material is possible using the parameters

$$C_*(f, f_\mu) = C_*(f, \tilde{F}_\mu), \tag{36}$$

$$F_*(f, f_\mu) = F_*(f, \tilde{F}_\mu), \tag{37}$$

$$\tilde{\sigma}_0(f, f_\mu) = \tilde{\sigma}_0(\tilde{F}_\mu). \tag{38}$$

The three-scale homogenization scheme is exemplified in Fig. 16. It shall be noted that the effective material law contains only three parameters: the micro-porosity f_μ, the microscopic yield stress of the incompressible matrix material σ_F and the mesoscale porosity f.

6 Summary and conclusions

A computational approach to the homogenization of isotropic porous materials with plastically compressible matrix material has been pursued. The computational homogenization methodology developed by [10] has been extended to the new material law. A wide range of plastic compressibility parameters $\tilde{F}$ and porosities f has been investigated. Results of previous studies have been taken into account in order to systematically reduce the computational effort which is still massive. More precisely a total of around 2,000 non-linear finite element simulations with periodic boundary conditions have been conducted. The asymptotic stress states are analyzed with the aim of (i) identification of an effective model for the non-linear porous material and (ii) providing data for comparison with current [e.g., 35] and future analytical models.

It was observed that the scatter of the computational results was rather small. This allows for two conclusions: (i) the microstructures and the loading conditions can be considered representative and (ii) a posteriori a smaller number of

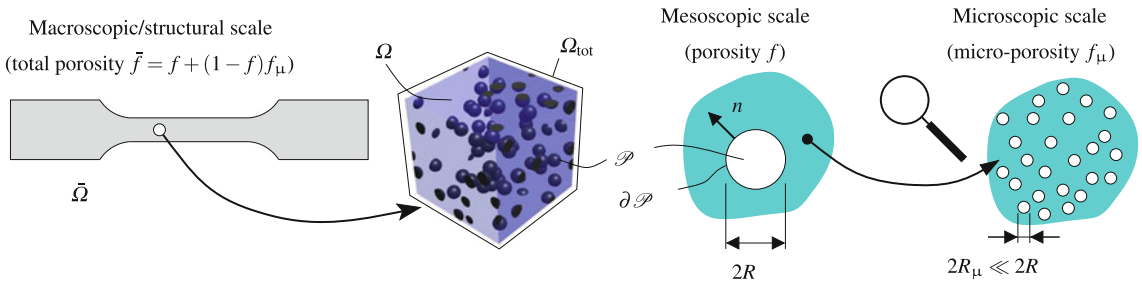

Fig. 15 Illustration of the three scale problem for double porous materials with mesoscopic pore radius R and microscopic pore radius $R_\mu \ll R$

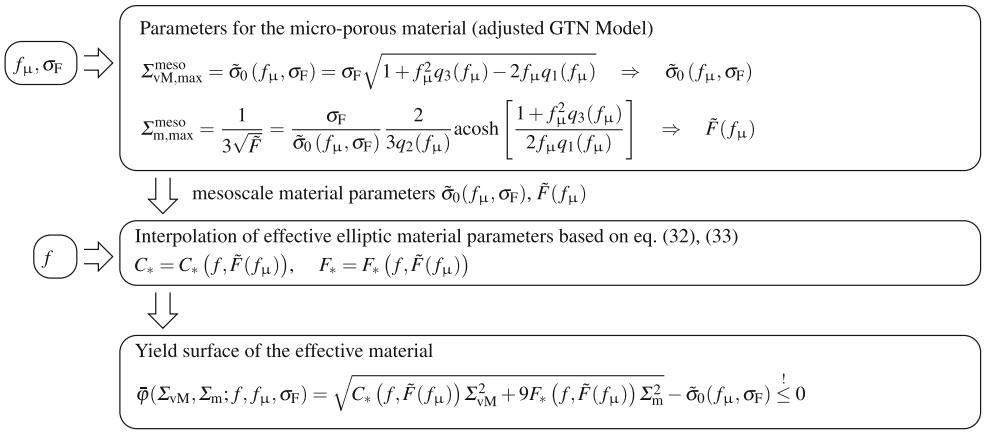

Fig. 16 Algorithm for the homogenization of the three-scale material consisting of two different size populations of voids (see Fig. 15)

variations might have been chosen at the expense of increased uncertainty.

Other than in the case of plastic incompressibility, the plastic volume change of the matrix material can amount for a substantial part of the total volume change. This fact is investigated in Sect. 3.3. It is found that depending on f and $\tilde{F}$ the amount of the volume change due to pore growth may vary considerably. Surprisingly the triaxiality of the macroscopic stress state has only a negligible influence on this effect. Further investigations can examine this aspect in more detail. In particular, the proposal of a possible growth criterion accounting for the matrix volume change is of interest, but beyond the scope of the current investigation.

Based on the numerical data it can be concluded that the effective material law can be approximated by an elliptic yield criterion with new parameters C_* and F_* which depend on the porosity f and the plastic compressibility $\tilde{F}$ on the microscale. An interpolation has been proposed and validated in Sect. 4. The simplicity of the approach and the wide range of admissible input parameters allow for an application of the model for many different materials, e.g., ductile foams, geomaterials or double porous materials as investigated by [35]. It shall be noted that the presented interpolation provides only one possible effective material law. The coefficients provided for the interpolated proposed model allow for a straight-forward use of the computational findings in simulations as well as for validation of model predictions in the future.

The application to a three-scale homogenization scheme of double porous materials is discussed in more detail in Sect. 5. The outcome of the proposed three-scale homogenization is an effective behavior that depends only on three parameters in a manageable format: the micro-scale porosity f_μ, the meso-scale porosity f and the yield stress σ_F of the solid phase on the lowest scale.

Acknowledgments Financial support of the French Agence Nationale de la Recherche (ANR) under reference ANR-BLAN08-1_321567 (Couphin project) and via the Gunther and Ingrid Schroff Stiftung related to the stay of F. Fritzen at the Centre des Matériaux (Evry, France) are highly acknowledged. Further, the authors gratefully acknowledge the valuable input of Prof. Marc Geers from TU Eindhoven (Netherlands) related to the plastic volume changes.

References

1. Badiche X, Forest S, Guibert T, Bienvenu Y, Bartout JD, Ienny P, Croset M, Bernet H (2000) Mechanical properties and non-homogeneous deformation of open-cell nickel foams: application of the mechanics of cellular solids and of porous materials. Mater Sci Eng A 289:276–288
2. Besson J, Abouaf M (1989) Behaviour of cylindrical HIP containers. Int J Solids Struct 28:691–702
3. Castañeda PP (2002) Second-order homogenization estimates for nonlinear composites incorporating field fluctuations: I—theory. J Mech Phys Solids 50(4):737–757
4. Danas K, Aravas N (2012) Numerical modeling of elasto-plastic porous materials with void shape effects at finite deformations. Compos Part B Eng 43(6):2544–2559
5. Danas K, Castañeda PP (2009) A finite-strain model for anisotropic viscoplastic porous media: I–theory. Eur J Mech A 28(3): 387–401
6. Danas K, Castañeda PP (2009) A finite-strain model for anisotropic viscoplastic porous media: II–applications. Eur J Mech A 28(3):402–416
7. Deshpande V, Fleck N (2000) Isotropic constitutive models for metallic foams. J Mech Phys Solids 48:1253–1283
8. Dirrenberger J, Forest S, Jeulin D (2012) Elastoplasticity of auxetic materials. Comput Mater Sci 64:57–61
9. Forest S, Blazy JS, Chastel Y, Moussy F (2005) Continuum modeling of strain localization phenomena in metallic foams. J Mater Sci 40:5903–5910
10. Fritzen F, Forest S, Böhlke T, Kondo D, Kanit T (2012) Computational homogenization of elasto-plastic porous metals. Int J Plast 29:102–119
11. Gărăjeu M (1995) Contribution à l'étude du comportement non linéaire de milieux poreux avec ou sans renfort. Ph.D. thesis, University of Marseille

12. Green R (1972) A plasticity theory for porous solids. Int J Mech Sci 14:215–224
13. Guo T, Faleskog J, Shih C (2008) Continuum modeling of a porous solid with pressure-sensitive dilatant matrix. J Mech Phys Solids 56:2188–2212
14. Gurson A (1977) Continuum theory of ductile rupture by void nucleation and growth: part I—yield criteria and flow rules for porous ductile media. J Eng Mater Technol 99:2–15
15. Jeong HY (2002) A new yield function and a hydrostatic stress-controlled model for porous solids with pressure-sensitive matrices. Int J Solids Struct 39:1385–1403
16. Jeong HY, Pan J (1995) A macroscopic constitutive law for porous solids with pressure-sensitive matrices and its implications to plastic flow localization. Int J Solids Struct 32(24):3669–3691
17. Lee J, Oung J (2000) Yield functions and flow rules for porous pressure-dependent strain-hardening polymeric materials. J Appl Mech 67:288–297
18. Lin J, Kanit T, Monchiet V, Shao JF, Kondo D (2010) Numerical implementation of a recent improved Gurson-type model and application to ductile fracture. Comput Mater Sci 47(4):901–906
19. Lubliner J (1990) Plasticity theory. Macmillan, New York
20. Maghous S, Dormieux L, Barthélémy J (2009) Micromechanical approach to the strength properties of frictional geomaterials. Eur J Mech A 28:179–188
21. McClintock F (1968) A criterion for ductile fracture by the growth of holes. ASME J Appl Mech 35:363–371
22. Michel J, Suquet P (1992) The constitutive law of nonlinear viscous and porous materials. J Mech Phys Solids 40(4):783–812
23. Monchiet V (2006) Contributions à la modélisation micromécanique de l'endommagement et de la fatigue des métaux ductiles. Ph.D. thesis, Université des sciences et Technologies de Lille, Lille
24. Monchiet V, Kondo D (2012) Exact solution of a plastic hollow sphere with a Mises–Schleicher matrix. Int J Eng Sci 51:168–178
25. Monchiet V, Charkaluk E, Kondo D (2011) A micromechanics-based modification of the gurson criterion by using eshelby-like velocity fields. Eur J Mech A 30:940–949
26. Nemat-Nasser S, Hori M (1999) Micromechanics: overall properties of heterogeneous materials. Elsevier, Amsterdam
27. Niordson CF (2008) Void growth to coalescence in a non-local material. Eur J Mech A 27(2):222–233. doi:10.1016/j.euromechsol.2007.07.001
28. Ponte-Castañeda P (1991) The effective mechanical properties of nonlinear isotropic composites. J Mech Phys Solids 39(1):45–71
29. Raghava R, Caddell R, Yeh G (1973) A macroscopic yield criterion for crystalline polymers. Int J Mech Sci 15:967–974
30. Raghava R, Caddell R, Yeh G (1973) The macroscopic yield behavior of polymers. J Mater Sci 9:225–232
31. Rice JR, Tracey DM (1969) On a ductile enlargement of voids in triaxial stress fields. J Mech Phys Solids 17:201–217
32. Schleicher F (1926) Zeitschrift für Angewandte Mathematik und Mechanik 6:199
33. Schöberl J (1997) Netgen an advancing front 2d/3d-mesh generator based on abstract rules. Comput Vis Sci 1(1):41–52
34. Shen W (2011) Modélisations micro-macro du comportement mécanique des matériaux poreux ductiles : application à l'argilite du Callovo-Oxfordien. Ph.D. thesis, University of Lille, Lille
35. Shen W, Shao J, Dormieux L, Kondo D (2012) Approximate criteria for ductile porous materials having a Green type matrix: Application to double porous media. Comput Mater Sci 62:189–194
36. Suquet P (1995) Overall properties of nonlinear composites: a modified secant moduli theory and its link with ponte castañeda's nonlinear variational procedure 320:563–571
37. Torquato S (2006) Random heterogeneous materials, 2 edn. Springer, Newq York
38. Tvergaard V (1981) Influence of voids on shear band instabilities under plane strain conditions. Int J Fract 17(4):389–407
39. Tvergaard V, Needleman A (1984) Analysis of cup-cone fracture in round tensile bar. Acta Metal 32:157–169
40. Vincent PG, Monerie Y, Suquet P (2009) Porous materials with two populations of voids under internal pressure: I. Instantaneous constitutive relations. Int J Solids Struct 46:480–506